applied sciences

MDPI

Article

Optimized Size and Distribution of Silver Nanoparticles on the Surface of Titanium Implant Regarding Cell Viability

Péter Hajdu [1,2,3,†], István Lampé [4,†], Richárd Rácz [1], Sándor Biri [1], Attila Csík [1], Ferenc Tóth [4], Melinda Szalóki [4], Viktória Hegedűs [4], Zsuzsanna Dombrádi [5], István Varga [6], István Csarnovics [2], Sándor Kökényesi [2], Dezső László Beke [7] and Csaba Hegedűs [4,*]

1 Institute for Nuclear Research (ATOMKI), Bem tér 18/c, H-4026 Debrecen, Hungary; hajdup@atomki.hu (P.H.); rracz@atomki.hu (R.R.); biri@atomki.hu (S.B.); csik.attila@atomki.hu (A.C.)
2 Faculty of Science and Technology Institute of Physics, University of Debrecen, Bem tér 18/a, H-4026 Debrecen, Hungary; csarnovics.istvan@science.unideb.hu (I.C.); kiki@science.unideb.hu (S.K.)
3 Doctoral School of Physics, University of Debrecen, Egyetem sqr. 1., H-4032 Debrecen, Hungary
4 Department of Biomaterials and Prosthetic Dentistry, Faculty of Dentistry, University of Debrecen, Nagyerdei Rd. 98, H-4032 Debrecen, Hungary; lampe.istvan@dental.unideb.hu (I.L.); ferenc.toth@med.unideb.hu (F.T.); szaloki.melinda@dental.unideb.hu (M.S.); hegedus.viktoria@dental.unideb.hu (V.H.)
5 Department of Medical Microbiology, Faculty of Medicine, University of Debrecen, Nagyerdei Rd. 98., H-4032 Debrecen, Hungary; dombradi.zsuzsa@med.unideb.hu
6 Department of Periodontology, Faculty of Dentistry, University of Debrecen, Nagyerdei Rd. 98, H-4032 Debrecen, Hungary; varga.istvan@dental.unideb.hu
7 Department of Solid State Physics, University of Debrecen, Bem tér 18/b, H-4026 Debrecen, Hungary; dbeke@science.unideb.hu
* Correspondence: hegedus.csaba.prof@dental.unideb.hu
† Péter Hajdu and István Lampé have contributed equally to this study as part of their Ph.D. work.

Received: 8 September 2020; Accepted: 9 October 2020; Published: 12 October 2020

Abstract: Though the antibacterial effect is advantageous, silver and silver nanoparticles can negatively affect the viability of human tissues. This study aims to check the viability of cells on surfaces with different particle size and to find the biologically optimal configuration. We investigated the effect of modified thickness of vaporized silver and applied heat and time on the physical characteristics of silver nanoparticle covered titanium surfaces. Samples were examined by scanning electron microscopy, mass spectrometry, and drop shape analyzer. To investigate how different physical surface characteristics influence cell viability, Alamar Blue assay for dental pulp stem cells was carried out. We found that different surface characteristics can be achieved by modifying procedures when creating silver nanoparticle covered titanium. The size of the nanoparticles varied between 60 to 368 nm, and hydrophilicity varied between 63 and 105 degrees of contact angle. Investigations also demonstrated that different physical characteristics are related to a different level of viability. Surfaces covered with 60 nm particle sizes proved to be the most hydrophilic, and the viability of the cells was comparable to the viability measured on the untreated control surface. Physical and biological characteristics of silver nanoparticle covered titanium, including cell viability, have an acceptable level to be used for antibacterial effects to prevent periimplantitis around implants.

Keywords: silver nanoparticles; antibacterial effect; periimplantitis; cell viability

1. Introduction

Titanium alloys are commonly used metallic materials in many fields of medicine for biomedical devices. Modern osseointegrated dental implants for restoring lost dentition are also made of

titanium [1]. Biocompatibility and prevention of inflammation around applied devices are essential for long term effectiveness [2]. The medical implant should be benign concerning the patients and should not cause a vicious immunological response. Commercially pure titanium (CpTi) is considered to be an ideal biocompatible dental material because of its surface properties as a result of the spontaneous growth of a stable and inert oxide layer [3]. CpTi is used primarily for endosseous dental implant applications [4]. Osseointegration of dental implants is described as a direct bone-to-implant contact [5]. Nowadays, it is an indispensable condition that an implant has to be a good bioinert material and also must have appropriate adhesion properties [6,7]. Osseointegration has four stages: hemostasis, inflammatory, proliferative, and remodeling. The very first step of the hemostasis phase is the development of a layer of a water-based solution containing inorganic and organic components that are essential for the osseointegration process [8]. Several works in literature present enhanced osseointegration with hydrophilic implant surface in native bone [9–11]. Pinotti et al. demonstrated improved osseointegration of titanium implants with hydrophilic surface in areas augmented with deproteinized bovine bone grafts and biphasic hydroxyapatite/beta-tricalcium phosphate grafts [12]. It was shown that, on a hydrophilic surface, a drop of water-based solution or blood spreads easily. CpTi is hydrophilic, thus it is essential that any modification of the surface should not decrease hydrophilicity. While many medical devices are embedded in the body and covered by tissues of the organ, dental implants are placed trans-gingivally, creating a potential gateway for bacteria to penetrate. This is a constant threat to developing inflammation called mucositis and periimplantitis [13]. The antibacterial feature of the implant surface at this gateway area can help to prevent this inflammation process [14]. One method of adding an antibacterial feature to the implant surface is silver layering [15–17]. Despite numerous investigations, the antibacterial effect of silver is still not fully understood, but it has long been a well-known and used material in medicine. Numerous studies prove that using silver nanoparticles (AgNPs) for layering significantly increases the antibacterial properties of the implants [18,19]. Silver ions tend to bond to sulphur, oxygen, and nitrogen [20] and thus to cell walls, membranes, DNA, enzymes, therefore altering their original functions [21,22]. On AgNP-Ti surfaces, reactive oxygen species are also generated to achieve additional antibacterial effects [18]. Surfaces with silver nanoparticles release silver ions that correlate with the surface. In a previous study, we demonstrated this antibacterial effect on a titanium surface covered by silver nanoparticles [23]. On the other hand, silver can be cytotoxic to human tissues by altering mitochondrial, DNA, membrane, and enzyme functions [24]. These mechanisms are the same as for bacteria, but for eukaryotic cells, a higher silver ion concentration is needed for comparable toxic effects. This opens up a therapeutic window for antibacterial treatment [25]. Controlling the diameter of the nanoparticles controls the total silver surface to release ions, thus the amount of ion can be controlled by the particle diameter.

This paper focuses on how the different sizes of silver nanoparticles affect the viability of human dental pulpal stem cells. Surface modification by using nanoparticles has an important role in the field of various research, especially in material science and medical applications [26–29]. By modifying the steps of surface treatment described in our previous study [23], we created surface configurations covered by differently sized silver nanoparticles. By culturing cells, their viability on the different surface configurations was investigated and compared. The optimal surface for cell growth was found for titanium dental implants covered by silver nanoparticles.

2. Sample Preparation

We used titanium substrates which were 15 mm diameter Grade 2 Titanium circular shape plates (99.6 at%, Grade 2). The plates were mechanically polished to #1200 grit level using Struers LaboPol-35 polishing machine with StruersLaboForce-Mi device (Struers, Copenhagen, Denmark), followed by chemical polishing with a corresponding proportional solution (silica gel: 5 mL; hydrogen peroxide: 0.77 mL; nitric acid: 0.02 mL; and hydrogen fluoride: 0.01 mL) for titanium to produce a mirror-like

surface. The substrates were then cleaned in acetone two times for 10 min each in an ultrasonic cleaning bath at room temperature, followed by rinsing with distilled water for 20 min and air drying.

To achieve a titanium surface covered by silver nanoparticles with different sizes, the pure titanium surface was modified in three stages:

Stage I—first annealing (I) of Ti samples to create TiO layer;

Stage II—applying physical vapor deposition (PVD) method to deposit silver layer with different thicknesses on Ti/TiO surface;

Stage III—second annealing (II) of Ti samples (already covered with Ti and Ag layers) at different temperatures for different times to achieve silver nanoparticles on the surface.

Creation of silver nanoparticles on titanium followed procedures described below.

2.1. Stage I: First Annealing

All samples were treated for 5 h at 550 °C to form a TiO_2 layer on the surface. With heat-treatment, the rutile phase is formed on the titanium surface, which allows the formation of a continuous silver layer and consequently, later on, the formation of silver nanoparticles [23]. In this way, a continuous silver layer can be deposited at room temperature and, by applying a further post-annealing under controlled conditions, different silver particle sizes (see Stage II) can be formed. The thickness of the formed oxide layer was measured by applying secondary neutral mass spectrometry (SNMS) method and was found to be 100 nm thick.

2.2. Stage II: Silver Deposition

The samples were covered with a thin silver film of different thicknesses including 3, 5, 8, and 15 nm, respectively. The silver layer was deposited by Bio-Rad E5000C type sputtering equipment from a pure (Goodfellow, 99.99%) silver target by applying argon (Ar) as the working gas. Sputtering parameters (deposition rate: 0,8 nm/s; sputtering current: 6 mA) were the same for all layer thicknesses, only the sputtering time was varied according to the layer thicknesses (3 nm: 12 s; 5 nm: 24 s; 8 nm: 48 s; 15 nm: 96 s).

2.3. Stage III: Second Annealing

The refined Brandon–Bradshaw model [30] describes that, in the case of nanocrystalline thin films, the continuous film layer breaks at the grain boundaries due to heat treatment. The time of the process depends on the layer thickness and the temperature. During annealing, grooves develop surface diffusion at the intersection of grain boundaries with the surface [31]. This process is driven by setting up the local equilibrium of the surface and the grain boundary energies. As time goes on, the free surface, created when the grooves reach the film–substrate interface, increases by surface diffusion, and the beaded surface forms. As a result of heat treatment in a vacuum furnace (300 °C, 400 °C, 500 °C, and 600 °C for 1 min) at Ar:H atmosphere, the continuous film is transformed to a discontinuous beaded film.

3. Experimental Methods

The samples before and after annealing were analyzed by applying different analytical methods.

3.1. Secondary Neutral Mass Spectrometry

Secondary Neutral Mass Spectrometry (SNMS) was used to examine the thickness of deposited silver layers. The analysis was carried out by an INA-X type SNMS system manufactured by SPECS GmbH, Berlin [32]. A 2 mm diameter circular-shaped area of samples was sputtered through a Ta mask. The sputtering time was converted to depth by measuring the sputtered crater by Ambios XP-I profilometer.

3.2. Scanning Electron Microscopy

The "cell-grown silver nanostructure" sample and the "non-cell-grown silver nanostructure" sample surfaces were examined by SEM (type JSM-IT500HR, produced by JEOL, Tokyo, Japan) equipped with energy dispersive X-ray (EDS) analyzer. In the case of "cell-grown silver nanostructure", samples were fixed with 2% (*v*/*v*) glutaraldehyde for 2 h and with 1% OsO_4 for 1 h, dehydrated using graded ethanol solutions (10, 30, 50, 70, 80, 90, and 100% (*v*/*v*), 15 min in each), and critical point dried using CO_2 before the examination by SEM. To prevent the charge accumulation on the surface, the samples were covered with a ~12 nm thick gold layer. The plasma current was 18–20 mA, while the sputtering Ar pressure was 10–20 MPa during the coating. Samples were analyzed by applying 10 kV accelerating voltage. To induce the characteristic X-ray emission for composition analysis, the 15 kV energy electron beam was applied.

3.3. Contact Angle Measurements

The sessile drop method was used to measure the water contact angle (CA) on silver covered and then beaded titanium surfaces by using DSA 30 Drop Shape Analyser (Krüss GmbH, Hamburg, Germany) at room temperature (25 °C). Drops of water (2 μL) were deposited on the top of the surface with an automatic dosing system (0.5 mm diameter needle). The contact angles were automatically calculated by fitting the captured drop shape to the degree calculated from the Young–Laplace equation. The average contact angle was determined from ten drops of the measurement ($n = 10$). The measured data were statistically analyzed by Student T-test ($p < 0.05$).

3.4. Cell Viability Assay

The cell viability on the different surfaces (polished Ti and Ti with different sizes of silver nanoparticles) was examined by Alamar Blue assay® (Thermo Scientific, Waltham, MA, USA) for dental pulp stem cells (DPSCs). Polished Ti samples were used as control. The 1×10^5 cells were seeded to the surface of the investigated samples and cultured for 14 days in DMEM F12 (Gibco, Waltham, MA, USA) supplemented with 10% (*v*/*v*) fetal bovine serum (FBS) (Gibco), 1% Glutamax (Gibco), and 1% Antibiotic-Antimycotic (Gibco). The culture medium was refreshed 3 times a week. Three samples were used for calculating the result for every measurement, as usual with biological samples. Alamar Blue assay was carried out according to the manufacturer's instructions; cell culture medium of each well was replaced with 10% (*v*/*v*) of Alamar Blue solution and, after 2 h of incubation at 37 °C in a humidified atmosphere with 5% CO_2, the fluorescence of samples (100 μL) were measured using a microplate reader (HIDEX Sense, Turku, Finland) at 544 nm excitation/595 nm emission.

4. Results

Figure 1 shows the difference between the individual silver layer thicknesses. The layer thicknesses were carefully selected to form four different types of AgNPs. As mentioned above, the difference between the average diameters of the nanoparticles created during heat treatment is to be clearly defined as a function of the layer thickness.

The deposition of silver layers was followed by several analyzing steps of the sample surface to control the size of the growing silver particles. After short, one minute heat treatment, the silver-deposited titanium samples were investigated by SEM to obtain a visual image of the beaded surface. Surface morphology was analyzed by applying National Instruments Visual Assistance image analysis program. We could obtain the number, the size (diameter), and even the distribution function of the silver nanoparticles changes in an area of about 9 μm^2.

The parameters of AgNPs preparation were varied by: (i) changing the thickness of the silver layer during the sputtering process (see Figure 1); (ii) changing the temperature during the heat treatment.

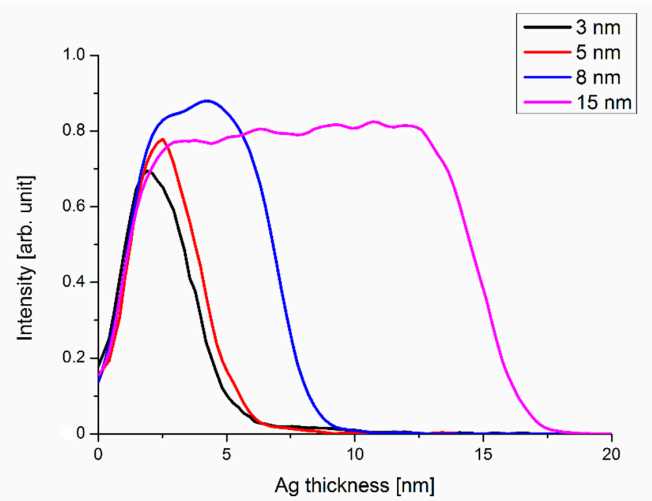

Figure 1. Depth profile of the four samples with different silver thicknesses measured by secondary neutral mass spectrometry (SNMS) method. The thickness of the layers was determined by the position of the half interface width obtained from the position of the distances between 90 to 10% decay of measured intensity.

In the case of fully beaded surfaces, there is a monotonic relationship between the diameter of the silver nanoparticles and the temperature of the heat treatment. The larger the amount of material deposited on the surface is, the larger were the nanoparticles that were obtained. It is also clear that, at thinner film thicknesses, the diameter of the nanoparticles is independent of the heat treatment temperature. By this method, silver nanoparticles of any average diameter can be produced between 40 and 400 nm (Figure 2). The cell growth investigations were performed at 600 °C heat-treated samples because, in this case, the nanoparticles were well separated, even after 1 min of heat treatment. The surface modification (Stages I, II, and III) of the samples was repeated on 24 samples. As a result, the difference in diameter between the AgNPs was visible depending on the thickness of the layers.

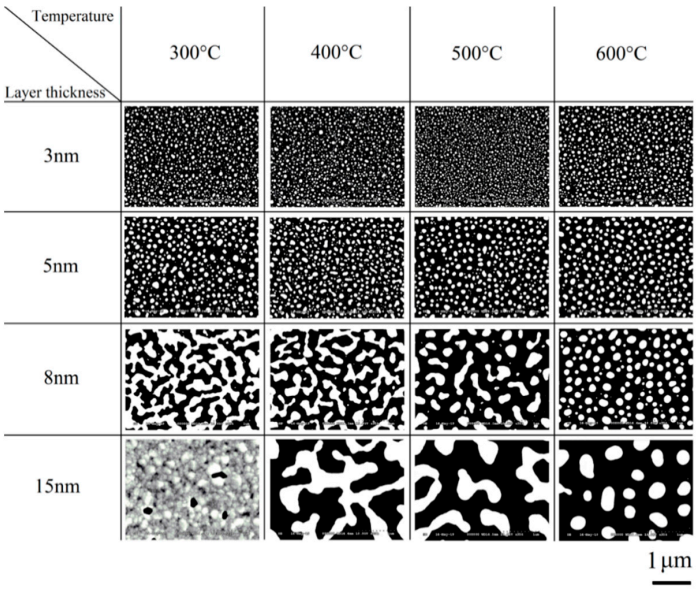

Figure 2. Scanning electron microscopy images taken of silver nanoparticles as a function of temperature and thickness of the deposited layer (see the details in the text).

The SEM image in Figure 3 shows the surface of a sample having an initial layer thickness of 15 nm before 600 °C 1 min heat treatment. The red spots in Figure 3B correspond to the Ag-L peak

and the green to the Ti-K peak, which are superimposed on the SEM image. The EDS mapping image (Figure 3B) is illustrated and colored into Figure 3C according to the peaks defined by EDS.

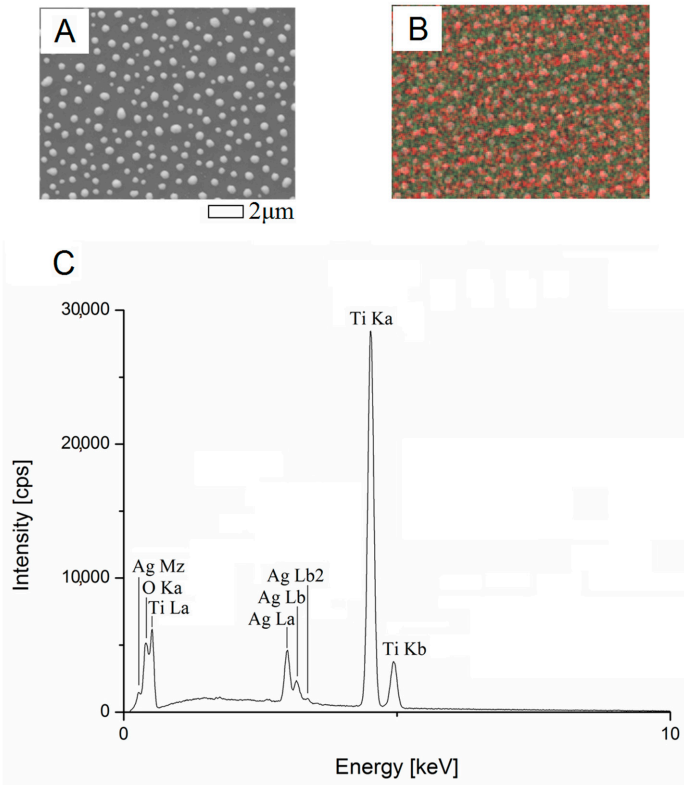

Figure 3. Scanning electron microscopy image (**A**) with the corresponding composition mapping image (**B**) and spectra (**C**). The typical characteristic lines of the elements are marked in the spectra.

Figure 4 shows how the size distribution of silver nanoparticles on the TiO surface changed as a function of the thickness of the silver layer previously sputtered on the surface. There is a linear relationship between the average diameter of the AgNPs and the thickness of the sputtered silver layer (see Figure 4B).

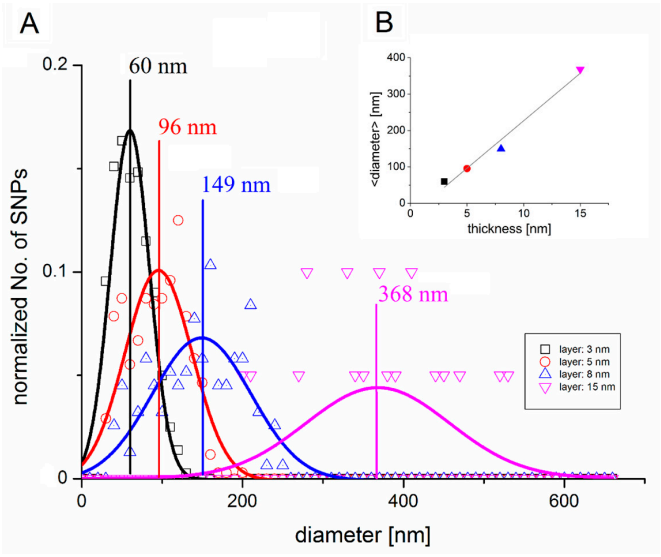

Figure 4. (**A**) Gaussian distribution of the average diameter of AgNPs; (**B**) linear relationship between average nanoparticle diameter and silver layer at T = 600 °C.

4.1. Contact Angle Measurements

The mean values of contact angle measurements are summarized in Figures 5 and 6. The water contact angles were 63.675° ± 0.608°, 66.275° ± 0.826°, 70.010° ± 0.667°, and 105.263° ± 0.823° at 60 nm, 96 nm, 149 nm, and 368 nm silver particle size, respectively. The water contact angles increased continuously with the size of the silver particles increasing.

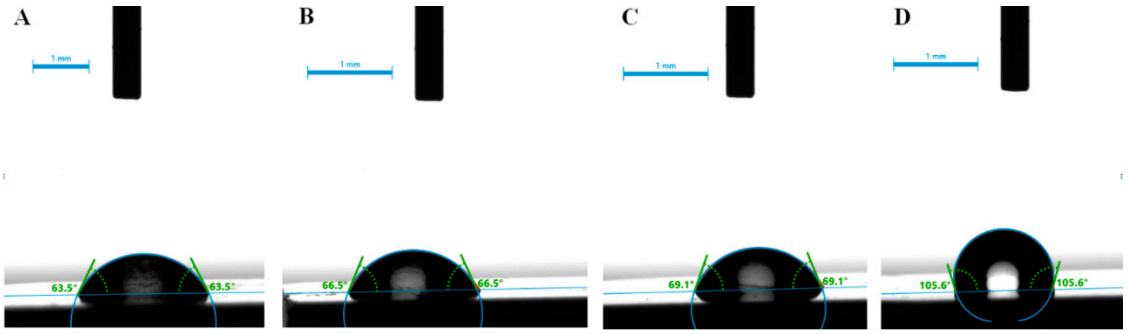

Figure 5. Representative pictures of water contact angle measurement on 60 nm (**A**), 96 nm (**B**), 149 nm (**C**), and 368 nm (**D**) silver nanoparticles modified titanium surface.

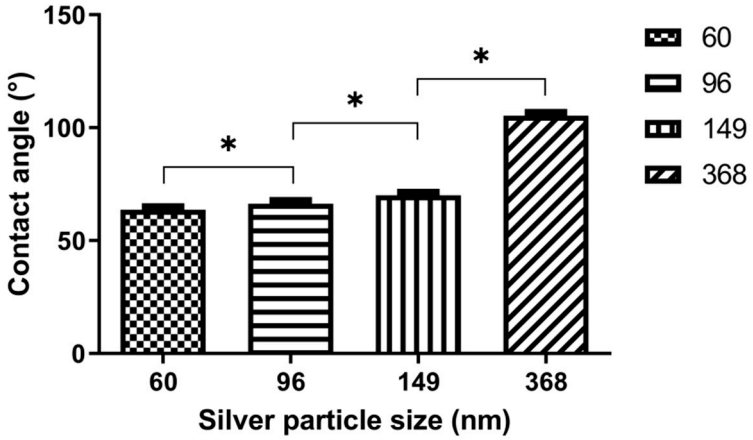

Figure 6. Mean values of water contact angle measurements of the four different silver particle size (* $p < 0.01$).

The mean contact angles of 60 nm, 96 nm, and 149 nm were below 90°, indicating the water behaved as a good wetting liquid on the tested surface, contributing to the hydrophilic nature of the modified titanium surface. With 368 nm sized silver particles, the mean contact angle was higher than the borderline value to demonstrate that the water behaved as a poor wetting liquid on the titanium surface covered by bigger silver particles. Moreover, the statistical analysis showed that the means differed significantly ($p < 0.01$) with increasing silver layer thickness.

4.2. Cell Growth

After 1 min heating at 600 °C, the nanoparticles were separated at each of the four films, and there was a well-defined difference between their average size distribution. Therefore, newer samples were prepared by the above-mentioned methods, but now only at 600 degrees. A total of 24 (4 × 6) samples were treated at 600 degrees. Eight control samples were used in the experiments. Cells were grown on each sample (Figure 7).

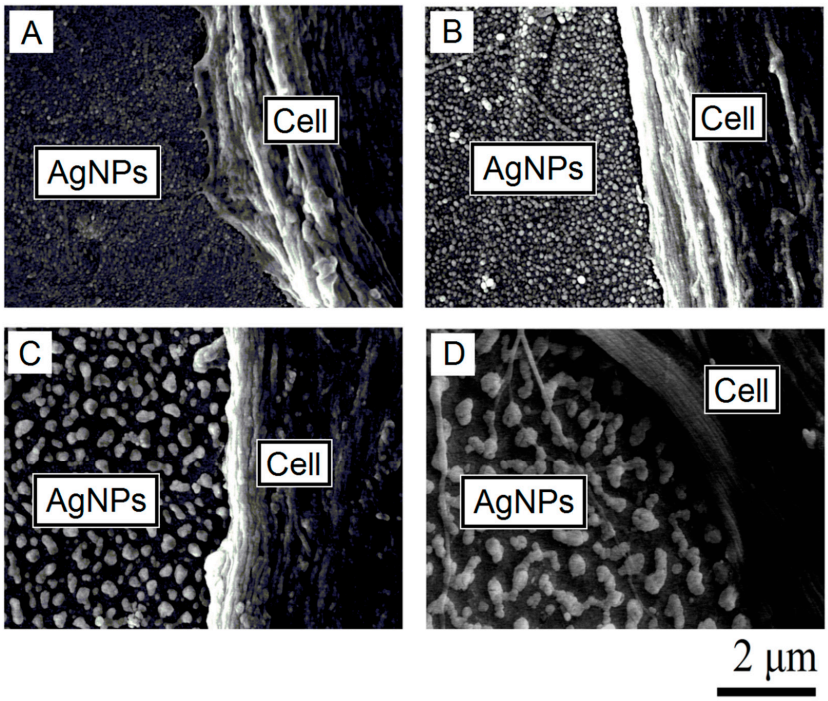

Figure 7. SEM images with nanoparticles of appropriate average diameter (**A**): 60 nm; (**B**): 96 nm; (**C**): 149 nm; (**D**): 368 nm and cell growth on them.

4.3. Cell Viability Assay

The cell viability on the superficial silver nanoparticles of different sizes was measured by Alamar blue assay. As a control, the cells were also seeded on to the surface of untreated, polished titanium surfaces.

After 14 days of culture, the cells seeded on surfaces covered by silver particles 60 and 96 nm in average diameter showed viability similar to the control surface. However, in the case of the surfaces covered with 149 and 368 nm average diameter silver particles, we observed monotonic reduction (Figure 8) of cell growth compared to the 60 nm particle surface. The viability of the cells grown on the 149 and the 368 nm particle surface was also reduced when compared to the 96 nm particle surface.

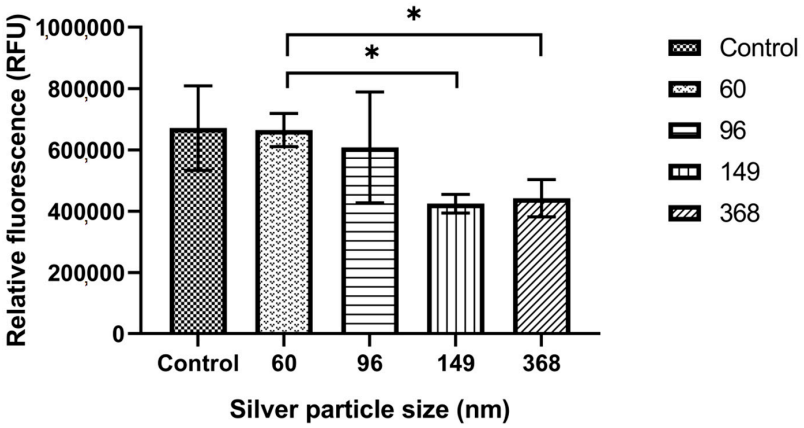

Figure 8. The effect of the diameter of superficial silver nanoparticles on the viability of dental pulp stem cells (DPSCs). Cells were seeded on silver nanoparticle covered titanium discs and cultured for 14 days. Cell viability was measured by Alamar Blue assay. Values are expressed as sample means, and error bars represent the standard deviations ($n = 3$). Statistically significant differences are indicated with asterisks (* $p < 0.01$).

5. Discussion

We investigated samples with different AgNP-Ti surface configurations as a result of different amounts of silver vaporized. Particle diameter, surface characteristics, cell viability, and hydrophilicity were compared. The nanoparticles created from 3 nm vaporized silver layers by heat treatment at 600 °C for 1 min had a good antibacterial effect, as we demonstrated in our former experiment [23] where the same 60 nm diameter silver nanoparticles were created and anchored to the titanium surface using electron cyclotron resonance (ECR) ion source. In this recent paper, we demonstrated that a surface with 60 nm silver particle diameter provided better viability for DPSCs than surfaces with a bigger particle diameter. Figure 8 shows that a layer with 100 nm or larger average nanoparticle size significantly decreased cell viability compared to 60 nm AgNP diameter.

The success of biomaterial and cell interaction is determined by many factors, from the part of the substratum properties to cell–substratum interactions. A few works also revealed that cell behavior is determined by not only surface properties but also cell type [33,34]. The influencing factors of surface properties such as surface hydrophilicity, roughness, texture, chemical composition of the substratum, charge, and others may be critical for the biocompatibility of the tested materials. Altankov et al. found that cell proliferation and substratum surface wettability are in direct relation (water contact angles were measured by the sessile drop method) [35]. Webb et al. studied the phosphate buffer contact angle on modified glass surfaces at different pH by the sessile drop method, and they found that hydrophilic surfaces (the better wetting ability by water) significantly enhance cell attachment and spreading. Moreover, cell attachment is influenced by wettability and charging of the surface [36]; hydrophilic surface and moderate surface hydrophilicity promoted cell attachment. Surface wettability can be analyzed with contact angle measurements that give information about surface hydrophilicity. The contact angle data are strongly influenced by surface characteristics such as chemical composition of the sample surface, surface topography, presence of entrapped air bubbles in surface irregularities, and chemical interaction between the liquid and the surface. In this investigation, the tested sample surface could be chemically considered as a heterogeneous (mixed) surface, where the Ag/titanium ratio changed after heat treatment. Moreover, a surface roughness diversity appeared with the Ag formed clusters (discontinuities) on the titanium surface, which meant an additional macro roughness surface to the nanotopography of the polished titanium surface. The water CA was around 83° on polished titanium (data not shown), and that value decreased to 63.675° after 60 nm AgNps were created on the surface (Figure 6). The water contact angle value increased up to 105° by increasing the size of AgNps to 368 nm. That can be explained by the change of Ag/Ti ratio on the actual surface, where the water was connected to the surface. The smaller Ag particles meant the presence of more AgNPs on the same sized testing area, which contributed to CA decreasing (from 83 to 63.675°) compared to unmodified Ti. The CA shifted to higher values with the increased Ag particle size, whereas Ag/Ti ratio decreased (smaller amount of Ag on the same size test area). Based on our measurements, it was found that the Ag/Ti ratio on the surface could also be determined by the shape and the size of silver nanoparticles. Meng F. et al. found a similar water contact angle on titanium surfaces, which was 89° [37]. In their study, the CA increased with silver deposition on the titanium surface, similar to our study findings.

In our study, the number of living cells was significantly greater on 60 nm and 96 nm silver particle-sized modified titanium surfaces, where the measured contact angle was lower than 70°. As the higher contact angle meant lower wetting ability, which can directly affect the adhesion of cells [38,39], we hypothesize that the observed reduction in cell number on the modified surfaces covered by 149 and 368 nm silver particles was directly associated with this phenomenon caused by the reduction of the interactive material surface. Data of this paper reveal that 60 and 96 nm particle sizes of AgNP do not significantly alter cell adhesion, which is a key clinical factor for successful dental implant therapy.

These features can play a high role in unambiguously identifying the exact silver nanoparticle diameter range created on the surface of titanium implants. However, due to another crucial factor, it is important to properly adjust the diameter of the nanoparticles; such a key consideration is economy. The amount of silver applied to the surface of the implants in clinical use is greatly influenced by

financial considerations, as it has become essential for the economical aspect to use the minimum amount of silver required. Thus, it became important to apply as little silver to the implants as is optimal for antibacterial effect, with the minimum amount of silver being used. Data reveal that silver nanoparticle coated titanium surfaces with 60 nm particle diameter have a good antibacterial feature, good biocompatibility, do not alter hydrophilicity, and contain less silver; thus, they may be optimal for dental practice in long-term use. Data also suggest that a bigger particle diameter decreases biocompatibility and cell viability and negatively alters hydrophilicity. Yang explains the phenomenon by the fact that it is due to the hydration layer formed around each AgNP that negatively affects the viability of the cells deposited on the surface [40]. The deposition of AgNPs on the titanium surface creates a surface that is increasingly hydrophilic depending on the decreasing size of AgNPs. This hydrophilic growth is greatly influenced by roughness of the surface [41], silver coverage, surface growth, and air bubbles on the surface trapped under the cells [38]. Another presentation of these two papers [38,41] is that AgNPs deposited to the surface are negatively charged, as shown in Figure 9 as an illustration. A multi-contact negative charge has a positive effect on hydrophilicity.

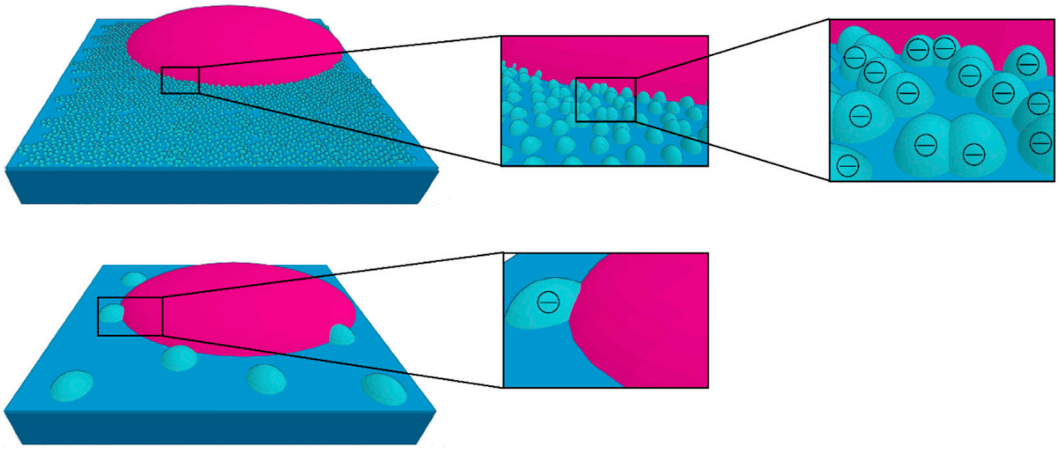

Figure 9. Schematic of 60 nm (upper) and 368 nm (bottom) average diameter silver nanoparticles (AgNPs) deposited onto titanium surfaces, on which cell culture was applied.

In summary, our research showed the diameter of the AgNPs formed as a function of the applied layer thickness and selected the diameter of the AgNPs as a function of the layer thickness, which was the least damaging to cell viability. Based on this, we can determine the amount of silver and the treatment necessary for these AgNPs to get the most optimal physical conditions for the highest cell viability.

6. Conclusions

In our study, we were able to produce silver nanoparticles of various sizes in a controlled manner from 40 to 400 nm. We showed that the smaller the formed AgNP size on the Ti surface is, the more hydrophilic the surface is. The negative charges of the AgNP can produce hydrophilic bubbles, and finally better adhesion with different peptides can be reached. We optimized the size of the AgNPs on the Ti surface to reach the best viable surface. Within the limits of this study, it can be presumed that the layer of AgNP with the size of 60 nm positioned cervically on dental implants can help to prevent periimplantitis without altering the viability of the adjacent cells.

Author Contributions: Conceptualization and headed the research, C.H., S.B., D.L.B. and S.K.; P.H., I.L. and M.S. designed and carried out most of the experiments. A.C. carried out SEM and EDS measurements. F.T. carried out cell viability tests. P.H., I.L. and C.H. wrote the manuscript, and all authors discussed the results and contributed to revisions. All authors have read and agreed to the published version of the manuscript.

Funding: The work is supported by the GINOP-2.3.2-15-2016-00011, the GINOP-2.3.2-15-2016-00022, and the GINOP-2.3.2-15-2016-00041 projects. Scanning electron microscopy measurements were performed with the support of the GINOP-2.3.3-15-2016-00029 project. The projects are co-financed by the European Union and the European Regional Development Fund. The research was financed by the Higher Education Institutional Excellence Programme (NKFIH-1150-6/2019) of the Ministry of Innovation and Technology in Hungary, within the framework of the Biotechnology thematic programme of the University of Debrecen.

Conflicts of Interest: The authors declare no conflict of interest.

References

1. Albrektsson, T.; Jacobsson, M. Bone-metal interface in osseointegration. *J. Prosthet. Dent.* **1987**, *57*, 597–607. [CrossRef]
2. Albrektsson, T.; Branemark, P.I.; Hansson, A.; Lindstrom, J. Osseointegrated Titanium Implants: Requirements for Ensuring a Long-Lasting, Direct Bone-to-Implant Anchorage in Man. *Acta Orthop. Scand.* **1981**, *52*, 155–170. [CrossRef] [PubMed]
3. Vishnu, J.; Manivasagam, V.K.; Gopal, V.; Garcia, C.B.; Webster, T.J. Hydrothermal treatment of etched titanium: A potential surface nano-modification technique for enhanced biocompatibility. *Nanomed. Nanotechnol. Biol. Med.* **2019**, *20*, 102016. [CrossRef] [PubMed]
4. Huang, J.; Zhang, X.; Yan, W.; Chen, Z.; Wang, Y. Nanotubular topography enhances the bioactivity of titanium implants. *Nanomed. Nanotechnol. Biol. Med.* **2017**, *13*, 1913–1923. [CrossRef] [PubMed]
5. Ferreira, A.M.; Tonda-Turo, C.; Mancuso, E.; Gentile, P. Multilayer nanoscale functionalization to treat disorders and enhance regeneration of bone tissue. *Nanomed. Nanotechnol. Biol. Med.* **2019**, *19*, 22–38. [CrossRef]
6. Özcan, I.; Uysal, H. Effects of silicon coating on bond strength of two different titaniumceramic to titanium. *Dent. Mater.* **2005**, *21*, 773–779. [CrossRef]
7. Puckett, S.; Webster, T. Control of osteoblast alignment on nano patterned titanium. *Nanomed. Nanotechnol. Biol. Med.* **2007**, *3*, 348. [CrossRef]
8. Ma, T.; Ge, X.-Y.; Zhang, Y.; Lin, Y. Effect of Titanium Surface Modifications of Dental Implants on Rapid Osseointegration. *Interface Oral Health Sci.* **2016**, 247–256. [CrossRef]
9. Chambrone, L.; Shibli, J.A.; Mercurio, C.E.; Cardoso, B.; Preshaw, P.E. Efficacy of standard (SLA) and modified sandblasted and acid-etched (SLActive) dental implants in promoting immediate and/or early loading protocols: A systematic review of prospective studies. *Clin. Oral Implant. Res.* **2014**, *26*, 359–370. [CrossRef]
10. Hinkle, M.R.; Rimer, S.R.; Morgan, M.H.; Zeman, P. Loading of titanium implants with hydrophilic endosteal surface 3 weeks after insertion: Clinical and radiological outcome of a 12-month prospective clinical trial. *J. Oral Maxillofac. Surg.* **2014**, *72*, 1495–1502. [CrossRef]
11. Lang, N.P.; Salvi, G.E.; Huynh-Ba, G.; Ivanovski, S.; Donos, N.; Bosshardt, D.D. Erarlyosseointegration to hydrophilic and hydrophobic implant surfaces in humans. *Clin. Oral Implant. Res.* **2011**, *22*, 349–356. [CrossRef] [PubMed]
12. Pinotti, F.E.; de Oliveira, G.J.P.L.; Aroni, M.A.T.; Marcantonio, R.A.C.; Marcantonio, E., Jr. Analysis of osseointegration of implants with hydrophilic surfaces in grafted areas: A Precilincal Study. *Clin. Oral Implant. Res.* **2018**, *29*, 963–972. [CrossRef] [PubMed]
13. Derks, J.; Tomasi, C. Peri-implant health and disease. A systematic review of current epidemiology. *J. Clin. Periodontol.* **2015**, *42*, 158–171. [CrossRef] [PubMed]
14. Kangwansupamonkon, W.; Lauruengtana, V.; Surassmo, S.; Ruktanonchai, U. Antibacterial effect of apatite-coated titanium dioxide for textiles applications. *Nanomed. Nanotechnol. Biol. Med.* **2009**, *5*, 240–249. [CrossRef] [PubMed]
15. Tallósy, S.P.; Janovák, L.; Ménesi, J.; Nagy, E.; Juhász, Á.; Balázs, L.; Deme, I.; Buzás, N.; Dékány, I. Investigation of the antibacterial effects of silver-modified TiO_2 and ZnO plasmonic photocatalysts embedded in polymer thin films. *Environ. Sci. Pollut. Res.* **2014**, *21*, 11155–11167. [CrossRef] [PubMed]
16. Hajkova, P.; Spatenka, P.; Krumeich, J.; Exnar, P.; Kolouch, A.; Matoušek, J.; Kočí, P. Antibacterial effect of silver modified TiO2/PECVD films. *Eur. Phys. J.* **2009**, *54*, 189–193. [CrossRef]
17. Li, H.; Cui, Q.; Feng, B.; Wang, J.; Lu, X.; Weng, J. Antibacterial activity of TiO_2 nanotubes: Influence of crystal phase, morphology and Agdeposition. *Appl. Surf. Sci.* **2013**, *284*, 179–183. [CrossRef]

18. Wang, G.; Jin, W.; Qasim, A.M.; Gao, A.; Peng, X.; Li, W.; Feng, H.; Chua, P.K. Antibacterial effect of titanium embedded with silver nanoparticles based on electron-transfer-induced reactive oxygen species. *Biomaterials* **2017**, *124*, 25–34. [CrossRef] [PubMed]
19. Joya, Y.F.; Liu, Z.; Joya, K.S.; Wang, T. Preparation and antibacterial properties of laser-generated silver-anatase nanocomposite film against Escherichia coli and Staphylococcus aureus. *Nanotechnology* **2012**, *23*, 495708. [CrossRef]
20. Song, H.Y.; Ko, K.K.; Oh, L.H.; Lee, B.T. Fabrication of silver nanoparticles and their antimicrobial mechanisms. *Eur. Cells Mater.* **2006**, *11*, 58.
21. Raffi, M.; Hussain, F.; Bhatti, T.M.; Akhter, J.I.; Hameed, A.; Hasan, M.M. Antibacterial characterization of silver nanoparticles against E. coli ATCC-15224. *J. Mater. Sci. Technol.* **2008**, *24*, 192–196.
22. Abbaszadegan, A.; Ghahramani, Y.; Gholami, A.; Hemmateenejad, B.; Dorostkar, S.; Nabavizadeh, M.; Sharghi, H. The effect of charge at the surface of silver nanoparticles on antimicrobial activity against gram-positive and gram-negative bacteria: A preliminary study. *J. Nanomater.* **2015**, *2015*, 1–8. [CrossRef]
23. Lampé, I.; Beke, D.; Biri, S.; Csarnovics, I.; Csik, A.; Dombrádi, Z.; Hajdu, P.; Hegedűs, V.; Rácz, R.; Varga, I.; et al. Investigation of silver nanoparticles on titanium surface created by ion implantation technology. *Int. J. Nanomed.* **2019**, *14*, 4709–4721. [CrossRef]
24. de Matteis, V.; Malvindi, M.A.; Galeone, A.; Brunetti, V.; Pompa, P.P. Negligible particle-specific toxicity mechanism of silver nanoparticles: The role of Ag+ ion release in the cytosol. *Nanomed. Nanotechnol. Biol. Med.* **2015**, *4*, 731–739. [CrossRef] [PubMed]
25. Alt, V.; Bechert, T.; Steinrucke, P.; Wagener, M.; Seidel, P. An in vitro assessment of the antibacterial properties and cytotoxicity on nanoparticulate silver bone cement. *Biomaterials* **2004**, *25*, 4383–4391. [CrossRef]
26. Racz, R.; Biri, S.; Hajdu, P.; Csik, A.; Vad, K.; Kökényesi, S.; Csarnovics, I.; Hegedűs, C.; Radics, T.; Bakó, J.; et al. Application of an ECR ion source for ionic functionalization of implant materials on the nanoscale. In *Proceedings of the 21st International Workshop on ECR Ion Sources (ECRIS2014)*; Institute of Applied Physics of the Russian Academy of Sciences: Nizhny Novgorod, Russia, 2014; ISBN 978-3-95450-158-8.
27. Csarnovics, I.; Hajdu, P.; Biri, S.; Hegedűs, C.; Kökényesi, S.; Rácz, R.; Csik, A. Preliminary studies of creation of gold nanoparticles on titanium surface towards biomedical applications. *Vacuum* **2016**, *126*, 55–58. [CrossRef]
28. Kökényesi, S.; Biri, S.; Hegedűs, C.; Csarnovics, I.; Csik, A. Functionalization of amorphous chalcogenide and titanium oxide layers by goldnanoparticles. *Adv. Mater. Res.* **2013**, *747*, 289–292. [CrossRef]
29. Racz, R.; Biri, S.; Csarnovics, I.; Kökényesi, S. Gold and calcium ion beams for materials research by the Atomki ECR Ion Source. *Acta Phys. Deb.* **2012**, *46*, 133–141.
30. Beszeda, I.; Beke, D.L.; Gontier-Moya, E.G.; Kaganovskii, Y.S.; Ianetz, D. Calculation of Surface Self-Diffusion Coefficients from AES Data on Decay of Thin Metal Films. *Defect Diffus. Forum* **2005**, *237*, 727–732. [CrossRef]
31. Mullins, W.W. Theory of Thermal Grooving. *J. Appl. Phys.* **1957**, *28*, 333. [CrossRef]
32. Vad, K.; Csik, A.; Langer, G.A. Secondary neutral mass spectrometry—A powerful technique for quantitative elemental and depth profilinganalyses of nanostructures. *Spectrosc. Eur.* **2009**, *21*, 13–17.
33. Oliveira, S.M.; Song, W.; Alves, N.M.; Mano, J.F. Chemical modification of bioinspired superhydrophobic polystyrene surfaces to control cell attachment/proliferation. *Soft Matter* **2011**, *7*, 8932–8941. [CrossRef]
34. Khor, H.L.; Kuan, Y.; Kukula, H.; Tamada, K.; Knoll, W.; Moeller, M.; Hutmacher, D.W. Response of cells on surface-induced nanopatterns: Fibroblasts and mesenchymal progenitor cells. *Biomacromolecules* **2007**, *8*, 1530–1540. [CrossRef]
35. Altankov, G.; Grinnell, F.; Groth, T.J. Studies on the biocompatibility of materials: Fibroblast reorganization of substratum-bound fibronectin on surfaces varying in wettability. *J. Biomed. Mater. Res.* **1996**, *30*, 385–391. [CrossRef]
36. Webb, K.; Hlady, V.; Tresco, P.A. Relative importance of surface wettability and charged functional groups on NIH 3T3 fibroblast attachment, spreading, and cytoskeletal organization. *J. Biomed. Mater. Res.* **1998**, *41*, 422–430. [CrossRef]
37. Meng, F.; Sun, Z. A mechanism for enhanced hydrophilicity of silver nanoparticles modified TiO2 thin films deposited by RF magnetron sputtering. *Appl. Surf. Sci.* **2009**, *255*, 6715–6720. [CrossRef]
38. Gittens, R.A.; Scheideler, L.; Rupp, F.; Hyzy, S.L.; Geis-Gerstorfer, J.; Schwartz, Z.; Boyan, B.D. A Review on the Wettability of Dental Implant Surfaces II: Biological and Clinical Aspects. *Acta Biomater.* **2014**, *10*, 2907–2918. [CrossRef]

39. Milleret, V.; Lienemann, P.S.; Gasser, A.; Bauer, S.; Ehrbar, M.; Wennerberg, A. Rational design and in vitro characterization of novel dental implant and abutment surfaces for balancing clinical and biological needs. *Clin. Implant. Dent. Relat. Res.* **2019**, *21*, 15–24. [CrossRef]
40. Yang, Z.; Guo, H.; Yao, Z.; Mei, Y.; Tang, C.Y. Hydrophilic Silver Nanoparticles Induce Selective Nanochannels in Thin Film Nanocomposite Polyamide Membranes. *Environ. Sci. Technol.* **2019**, *53*, 5301–5308. [CrossRef]
41. Cai, S.; Bhushan, B. Meniscus and viscous forces during separation of hydrophilic and hydrophobic smooth/rough surfaces with symmetric and asymmetric contact angles. *Philos. Trans. R. Soc. A* **2008**, *366*, 1627–1647. [CrossRef]